Minable coal reserve estimation by incorporating tonnage and calorific value uncertainties by successive multiple-point and two-point geostatistical simulation algorithms

by F. Suparno[1,2], A. Paithankar[1], S. Chatterjee[1]

Affiliation:
[1]Department of Geological and Mining Engineering and Sciences, Michigan Technological University, USA
[2]Mining Engineering Study Program, University of Jember, Indonesia

Correspondence to:
S. Chatterjee

Email:
schatte1@mtu.edu

Dates:
Received: 4 Dec. 2024
Revised: 7 Mar. 2025
Accepted: 31 Jul. 2025
Published: September 2025

How to cite:
Suparno, F., Paithankar, A., Chatterjee, S. 2025. Minable coal reserve estimation by incorporating tonnage and calorific value uncertainties by successive multiple-point and two-point geostatical simulation algorithms. *Journal of the Southern African Institute of Mining and Metallurgy,* vol. 125, no. 9, pp. 555–570

DOI ID:
https://doi.org/10.17159/2411-9717/3448/2025

Abstract

Estimating reserves and quantifying resources stand as pivotal and intricate endeavours within the realm of coal mining operations. Intricate geological formations compound the challenges in resource estimation, thereby complicating reserve calculations. The uncertainties tied to geological attributes of coal, encompassing parameters like tonnage and coal quality, wield significant sway over resource and reserve computations within coal mines. This research delves into the domain of geological uncertainties, with a specific focus on calorific value, aiming to numerically characterise resources and reserves within an open-pit coal mine situated in Indonesia. To quantify resources, the coal seam geometry underwent simulation via a multi-point geostatistical technique known as single normal equation simulation. A geologically established coal seam served as the training image for generating 20 equiprobable coal models. To simulate CV, 50 realisations were generated for each simulated coal seam, utilising sequential Gaussian simulation. Deviations of the simulated coal seams ranged from -0.07% to 5.48% in comparison to the training image. The CV simulation yielded an average value of 5,920.29 kcal/kg, accompanied by a standard deviation of 586.54 kcal/kg. However, the average CV spanned from 5,305.26 kcal/kg to 6,526.55 kcal/kg across diverse simulations. For reserve calculation within the context of geological uncertainties, an algorithm rooted in maximum flow graph theory was employed to construct the ultimate pit for the coal mine. Within this final pit, the average stripping ratio was 1.62, coupled with a CV value of 6,019.66 kcal/kg. When juxtaposed with the deterministic model, the findings underscore that the stochastic ultimate pit delineates a more expansive excavation, accompanied by a heightened undiscounted cash flow.

Keywords

mineral resource, coal, open-pit, geostatistics, calorific value, uncertainty

Introduction

A mining operation constitutes a substantial investment commitment aimed at extracting valuable materials, such as coal, from the subsurface using either open-pit or underground methods. Within the coal industry, like other sectors encompassing metal and non-metal mining, investment decisions are grounded in meticulous assessments of economic coal reserves. Prior exploration drilling and consequent geological analyses determine key physical attributes, encompassing size, shape, and grade (such as calorific value) of a coal deposit. This process yields distinct units of established size, each possessing specific properties, such as tonnage and calorific value, known as mining blocks. These mining blocks exhibit economic value if deemed ore, while those without such value are categorised as waste (Asad, Dimitrakopoulos, 2013). In the coal realm, ore equates to coal seams, and waste corresponds to overburden (OB). The intricate nature of coal seams, marked by heterogeneous calorific values and other geological factors, exacerbates the challenges in resource estimation (Heriawan, Koike, 2008). Notably, uncertainties tied to resource estimation resonate with unpredictable raw material supply from mining operations (Tercan et al., 2013).

The assumption of constant economic values for mining blocks, neglecting the uncertainties in resource estimation (termed geological risk), can spawn impractical mine designs and financial losses (Dimitrakopoulos et al., 2002; Godoy, Dimitrakopoulos, 2011). This geological risk stands as a primary reason for falling short of production targets. The consequences of disparities between plans and actual outcomes have been explored by Dimitrakopoulos and Godoy (2014). Technical risks in coal mining predominantly arise from uncertainties in calorific value (CV), tonnage, and geo-mechanical aspects

(Tercan, Sohrabian, 2013; Zhang et al., 2018). Addressing these uncertainties and integrating them into the optimisation process is pivotal for establishing resilient coal mine plans and designs.

The characteristics of coal deposits, including size, calorific value, and shape, remain latent until extraction commences (Camus, 2002). Conventional methods often generate inaccurate solutions by disregarding uncertainties, potentially leading to future complications during mining operations. These methods rely on a singular coal resource model, estimating CV through kriging (Siddiqui et al., 2015) and tonnage through geologist-developed solid coal seam models or wireframes. Yet, a single resource model realisation from a geologist may inadequately estimate the true deposit volume (Heriawan, Koike, 2008). Tonnage uncertainty can result in discrepancies between planned and actual production in mines (Goodfellow, 2012). Goodfellow (2012) asserts that incorporating tonnage and grade uncertainties into mine planning markedly enhances resource and reserve estimation. To address tonnage uncertainty, approaches like indicator-based two-point variogram-based geostatistics (Heriawan, Koike, 2008) or multiple-point statistics (Abulkhair, Madani, 2022) are employed. However, limitations of the two-point variogram-based geostatistics are well-documented, particularly for categorical data simulation (Journel, Zhang, 2006).

Multi-point statistics (MPS) have limited application in the mining industry, especially for simulating sedimentary deposits like coal. Nevertheless, MPS has found success in modelling other commodities. Osterholt and Dimitrakopoulos (2007) utilised the single normal equation simulation (SNESIM) algorithm to capture lithological model uncertainties in the Yandi channel iron ore deposit. Chatterjee et al. (2012) employed wavelet-based methods to simulate rock types in the Olympic Dam deposit. Goodfellow et al. (2012) combined multi-point and two-point simulations for orebody models and grade uncertainty. Paithankar and Chatterjee (2018) used multi-point statistic simulations to model volume uncertainty and sequential Gaussian simulation for grade uncertainty in a copper deposit. MPS's application to coal mine tonnage uncertainty analysis has been documented only by Abulkhair and Madani (2022). Bastante et al. (2008) conducted a comparative study of indicator kriging (IK), sequential indicator simulation (SISIM), and single normal equation simulation (SNESIM) for uncertainty analysis of slate resource estimation.

Another paramount uncertainty, especially in resource modelling, stems from mineral grade. In the mining industry, grade elucidates the quality of mining commodities. For coal mining, coal quality is characterised by parameters like CV, ash content, volatile matters, and sulfur content. Traditional methods have often been employed for coal resource estimation (Saikia, Sarkar, 2013; Afzal, 2018), but these overlook uncertainty factors, potentially leading to discrepancies between plans and actual production (Rendu, 2002). Commonly used methods like kriging exhibit limitations, overestimating low-value samples and underestimating high-value ones, thereby making them unsuitable for quantifying uncertainty (Goovaerts, 1997). Conditional simulation (CS), a Monte Carlo-based method, addresses kriging's drawbacks (Pyrcz, Deutsch, 2014). CS, particularly sequential Gaussian simulation (SGS), is employed to model uncertainties, particularly spatial attributes like CV (Heriawan, Koike, 2008). In conditional simulation, the existence of a geological unit at any coal body location is modelled as a discrete random variable. Heriawan and Koike (2008) employed sequential Gaussian simulation to assess risks tied to coal quality parameters. Tercan and Sohrabian (2013) used independent component analysis and Gaussian simulation to explore uncertainties in multiple coal quality parameters. Yüksel et al. (2017) combined geostatistical simulation and Kalman filtering to update coal resource models and quantify uncertainty. Sohrabian et al. (2023) utilised a simulated annealing-based approach for multivariate coal quality parameter simulation.

Reserve estimation is a pivotal step in assessing the economic viability of mining operations. The Canadian Institute of Mining, Metallurgy, and Petroleum (CIM) defines mineral reserves as economically mineable portions of measured or indicated mineral resources substantiated by preliminary feasibility studies (CIM, 2014). In open-pit mining, calculating mineable reserves hinges on appropriately designing the ultimate pit for production planning (Kumar, Chatterjee, 2017). Various researchers have applied geostatistical and optimisation methods to estimate minable coal reserves for both open-pit and underground mines (Moore, Friederich, 2021; Dimitrakopoulos, Li, 2010). Amini et al. (2022) applied a stochastic optimisation algorithm for coal blending to reduce supply chain risk. Stevanovic et al. (2014) utilised stochastic programming to ensure a consistent coal supply from the mine to the power plant, aiming to minimise sulfur emissions and maximise calorific value. Wang et al. (2025) considered uncertainties in coal quality parameters to determine coal mine production capacity. Although many studies have incorporated coal quality uncertainties, to the best of our knowledge, none have integrated both volume and coal quality uncertainties for minable coal reserve estimation.

In this study, two major geological uncertainties – coal volume and calorific values – were integrated to quantify resources and reserves in an Indonesian coal mine. The single normal equation simulation (SNESIM), a multi-point geostatistical approach, was employed to capture volume uncertainty, while sequential Gaussian simulation (SGS) was used to quantify uncertainty associated with calorific value. A stochastic graph-cut method was implemented, incorporating both uncertainties to quantify coal reserves for the studied mine. The innovative aspect of this research lies in the integration of MPS with two-point geostatistics, which can significantly enhance resource quantification, and the stochastic graph-cut algorithm, which can generate robust reserves under multiple geological uncertainty conditions.

Methodology

Multiple-point geostatistical simulation and two-point conditional simulation were used to quantify the volume and calorific value uncertainty, respectively. The multi-point simulation, (MPS) (Strébelle, 2002), was utilised to generate the coal body model's resulting volume uncertainty. After generating the shapes of the coal body, the two-point conditional simulation for the calorific value uncertainty started through sequential Gaussian simulation (Deutsch, Journel, 1998). Figure 1 shows the flowchart of the successive simulations adopted in this research. After quantifying the resource model, the reserve was calculated by using the maximum flow minimum cut algorithm (Chatterjee et al. 2016; Asad, Dimitrakopoulos, 2013). The methodology of the proposed research is presented in three different sub-sections: (a) quantification of volume uncertainty; (b) quantification of calorific value uncertainty; and (c) reserve quantification under volume and calorific value uncertainties.

Quantification of volume uncertainty

For quantifying volume uncertainty, the SNESIM algorithm was implemented. Initially introduced and formulated by Strébelle

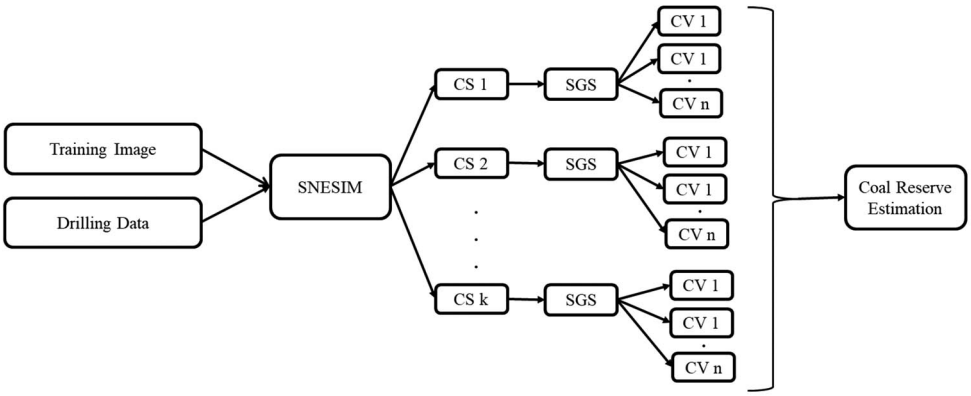

Figure 1—Flowchart of the proposed method

(2002), the SNESIM algorithm utilises a training image to establish probability patterns for the simulation process. A training image can be perceived as a representation of the spatial distribution of the deposit. Although a training image might not encompass exhaustive precision regarding deposit information, it does encapsulate the underlying geological context, thereby depicting the intricate complexity and heterogeneity that the deposit exhibits. In certain scenarios, a limited number of training images exist, with each individual image portraying differing levels of complexity and heterogeneity in geological interpretations. Consequently, during the simulation process, conditioning data are employed to regenerate the original data's values at their respective locations, thus fostering the creation of spatial continuity.

Assuming a categorical property S, having K possible states, $\{s(k),k = 1,\ldots,K\}$. A data event d_n of length n at centre location of u has a geometric pattern of the vector $\{h_\alpha,\alpha = 1,\ldots, n\}$ and the values of the data $\{s(u + h_\alpha), \alpha=1,\ldots,n\}$. The geometric template τ_α is correlated to the data template τ_n that saves the previous data geometry and data event d_n. In this paper, $K = 2$ because there are only 2 states, either coal or overburden.

SNESIM operates by sequentially simulating grids along a randomised pathway, originating from a random node during a single iteration (Huang et al., 2013; Strébelle, Journel, 2001). The node previously visited and simulated assumes the role of hard data and serves as the foundation for the conditional simulation of the following node in the subsequent sequence. The probability of data events, denoted as d_n, is determined by the multi-point statistics. The expression for the conditional probability of state s_k at location u is formulated as follows:

$$Prob\{s_k|S(u_\alpha), \alpha = 1, \ldots, n\} \text{ or } Prob\{S(u) = s_k|d_n\} \quad [1]$$

where d_n indicates the conditioning data event constructed by the n closest data, $(u + h_\alpha)$, $\alpha = 1, \ldots, n$. The training image can infer the probability of occurrence of data event d_n with data template τ_n. By utilising Bayes's relation, the probability distribution conditional to d_n, which is the category proportions gained from the central values of the training d_n, can be calculated using Equation 2:

$$Prob\{S(u) = s_k|d_n\} = \frac{Prob\{S(u)=s_k \text{ and } d_n\}}{Prob\{d_n\}} = \frac{c_k(d_n)}{c(d_n)} \quad [2]$$

where $Prob\{d_n\}$ is estimated by combining the scanned training image and the number $c\,(d_n)$ of training images, which reproduce the same properties of the conditioning data event d_n, and $Prob\{S(u)=s_k$ and $d_n\}$ can be estimated by calculating the number $c_k\,(d_n)$ of those which reproduce the same properties among the previous $c(d_n)$, related to a central value $S(u)$ equal to s_k. The concept of a search tree in SNESIM can be helpful to calculate directly the conditional probability in Equation 2. A 4x4 binary training image is shown in Figure 2(a). Figure 2(b) represents a template τ_n, with $n = 4$ for conditioning data. Then, a search tree, as illustrated in Figure 2(c), can be constructed by searching for the data template in the training image. In the search tree, the root node (level 0) displays the frequency of coal (7) and OB (9) in the training image. At level 1 of the search tree, the left-hand branch shows that the frequency of the central node (u) being OB and the top node (u_1) being coal is 2, while the frequency of the central node being coal and the top node being OB is 3. These values are used to calculate the conditional probability of the central node given that the value of the u_1 node is coal. In this case, the conditional probability of the central node being coal, given that u_1 is coal, is 0.6 (3 out of 5), and the probability of it being OB is 0.4 (2 out of 5). As one moves further down the search tree, more conditioning data become available, allowing for the calculation of increasingly specific conditional probabilities for the simulation. From Equation 2, the conditional probability can be directly retrieved from various levels of the search tree, relying on the number of the conditional data.

The SNESIM algorithm strategically relies on a single normal equation (SNE) (Equation 2) during the computation of coal and overburden probabilities at specific grid nodes, contributing to its expedited execution. In SNESIM, the SNE is a conceptual term that refers to how the conditional probability distribution of categorical variables is calculated, as shown in Figure 2. Unlike a comprehensive kriging system, SNESIM's internal method enables the direct calculation of probabilities using a single normal equation, determining proportions between relevant variables without calculating a variogram and solving a kriging system of equations (Arpat, Caers, 2007; Strébelle, Journel, 2001). For a specified data template τ_n, the central values $c_k\,(d_n)$ over the training image and number of occurrences $c(d_n)$ of the data events d_n are saved in a search tree, where the training proportions can be identified.

A scenario arises when the proportion of simulated coal and overburden in the target deposit deviates from that of the training image. To address this, Strébelle (2002) and Liu (2006) employed a servosystem control mechanism aimed at aligning the proportion of simulated categories as closely as feasible to the target category proportion during the simulation of specific nodes, for example, considering the proportion of the training image as $P(A)$, where A

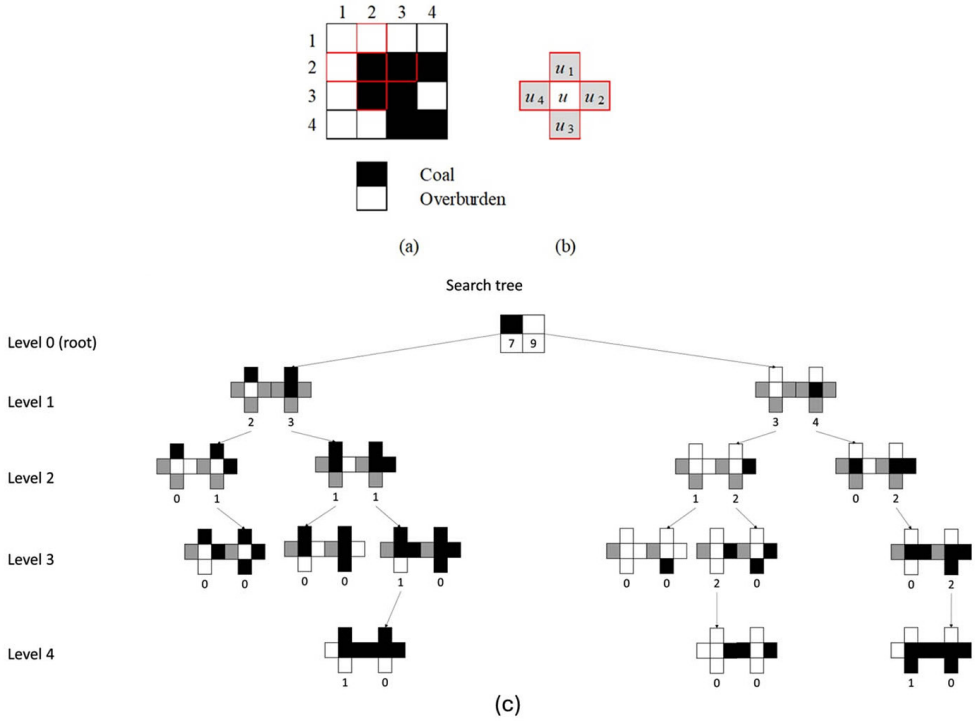

Figure 2—Example of (a) 4x4 size training image, (b) data template, and (c) search tree

indicates lithology indicators and the target lithology proportion is represented as $P(A^*)$. After simulations, $P(A)$ and $P(A^*)$ hold very dissimilar lithology proportions, and the target lithology proportion $P(A^*)$ cannot be properly reproduced, so a servosystem control is then applied to fix the problem.

Assume $P^c(A)$ is the current probability distribution function before taking a simulation of the unknown node u. To achieve the goal of the target lithology proportion $P(A)$, a conditional probability $P(A|B)$ is adjusted to:

$$P^{new}(A|B) = P(A|B) + \mu\big((P(A) - P^c(A)\big) \quad [3]$$

where μ is obtained by using the servosystem control λ, as stated in the following:

$$\mu = \frac{\lambda}{1-\lambda}, \lambda \in [0,1] \quad [4]$$

The value of $\lambda$is directly proportional to μ.

The work flows of the SNESIM algorithm are stated as follow:

- Use data template to scan the training image.
- Collect the occurrences of all data events d_n and save them in the search tree.
- Define a random path to visit all the nodes to be simulated.
- Simulate each node by following these steps:
  - Take the data events d_n from the search tree subject to hard condition data.
  - Given surrounding data events d_n, compute the occurrence probability of the data event using Equation 2.
  - Update the conditioning data by adding the previously simulated node to the grid.
- Run for a select number of simulations.

Calorific value uncertainty

Subsequent to coal volume simulation, the simulation of calorific value was conducted for each of the simulated coal body models. The SGS was the method employed for the simulation of calorific value. Initially introduced by Deutsch and Journel (1998), SGS has demonstrated effectiveness in reproducing structured statistics on a global scale, notably variograms. In contrast, the kriging method is recognised for providing locally accurate estimates at each specific location. The formula of variogram as a vector $\gamma(h)$ calculation is given in Equation 5:

$$\gamma(h) = \frac{1}{2N(h)}\sum_{\alpha=1}^{N(h)}[Z(u_\alpha) - Z(u_\alpha + h)]^2 \quad [5]$$

where $N(h)$ is the number of points separated by distance vector h, and $Z(u_\alpha)$, $Z(u_\alpha+h)$ are calorific values at location u_α and $u_\alpha+h$, respectively.

SGS achieves the replication of spatial attributes by utilising conditional distribution functions. During each iteration where N nodes are randomly traversed, a conditional cumulative distribution function (CCDF) is established and subsequently sampled. Assuming a set of N random variables $Z(u_\alpha)$, $\alpha = 1, \ldots, N$ specified at N locations u_α the multivariate N point CDF of stationary random fields can be formulated as an output of N univariate CCDFS:

$$\begin{aligned} &F\big(u_1, \ldots, u_N; z_1, \ldots, z_N \big| (n)\big) = \\ &F\big(u_N; z_N \big| (n+N-1)\big)\ \mathrm{x} \\ &F\big(u_{N-1}; z_{N-1} \big| (n+N-2)\big)\ \mathrm{x} \ldots \mathrm{x} \\ &F\big(u_2; z_2 \big| (n+1)\big)\ \mathrm{x}\ F\big(u_1; z_1 \big| (n)\big) \end{aligned} \quad [6]$$

where $F(u_N;z_N|(n+N-1))=Prob\{Z(u_n)\leq z_N|(n+N-1)\}$ represents the conditional distribution function of $Z(u_N)$ for the group of n original data values and $(N-1)$ represents the prior simulated values.

The reproduction of the variogram model is achieved by constructing each CCDF using both n data and previously simulated values. Within the context of SGS, an assumption is made that the local CCDF follows a standard normal distribution;

otherwise, the initial z data must be transformed into y-values conforming to a standard normal distribution. This transformation, known as the normal score transformation, is executed by associating the corresponding percentiles of the cumulative distribution of Z with those of the standard normal distribution. Importantly, this transformation preserves the rank order of the original data. Fundamentally, the SGS approach leverages simple kriging to perform simulation within the normal score space, where deviations from the random normal score are expressed as follows:

$$y = \mu_{SK} + r\sigma_{SK} \quad [7]$$

$$\mu_{SK} = E\{Z(u)\} \quad [8]$$

$$\sigma_{SK} = \sqrt{Var\{Z*(u) - Z(u)\}} \quad [9]$$

where μ_{SK} represents the kriging mean, σ_{SK} represents the kriging variance, r represents the random number [0,1], and $Z*(u)$ represents the estimated value. The final step is back-transforming the realisations/result (Deutsch, Journel, 1998; Goovaerts 1997). The workflow of the SGS is stated below:

- Transform into normal score $Z(u)$ from the original data $Y(u)$.
- Use a defined random path to visit each node and simulate.
- For each node u_α, $\alpha = 1, \ldots, N$:
  - Model the conditional distribution $F(u_\alpha; z_\alpha|(n + \alpha - 1))$ of $Z(u_\alpha)$, provided the n original data values and $\alpha - 1$ prior to simulated values.
  - Plot the simulated value from $F(u_\alpha; z_\alpha|(n + \alpha - 1))$.
- After visiting all the nodes, do back transformation of the simulated nodes into the original variables.

Coal reserve calculation under uncertainties

The Canadian Institute of Mining, Metallurgy, and Petroleum (CIM) defines mineral reserves as the economically viable portion of a mineral resource, substantiated through a feasibility study (CIM, 2014). Within the context of open-pit mining, the mineable reserve encompasses a subset of the mineral resource situated within the ultimate pit boundary (Chatterjee et al., 2016; Kumar, Chatterjee, 2017). For calculation of the ultimate pit, the maximum flow minimum cut algorithm is employed. This algorithm tackles the challenge of identifying the most extensive closure within a mine graph, where the minimum cut delineates an optimal pit contour (Hochbaum, 2001). The subsequent mathematical formulation was adopted for the calculation of the minable reserve:

Objective function:

$$Maximize \sum_{\gamma \in \Gamma} . \sum_{b \in B} . \ v_{\gamma b} x_b \quad [10]$$

$$x_b - x_{b'} \leq 0. \quad b' \epsilon \xi_b. \quad b \epsilon B$$
$$x_b \ \epsilon \{0,1\}. \quad b \epsilon B. \quad [11]$$

where $v_{\gamma b}$ is the economic value of a coal mining block b from simulation, x_b is the binary decision variable, which takes value 1 if mining block b is inside the pit and 0 otherwise, b' is the block that needs to be mined before mining block b to satisfy slope constraints, Γ is the number of simulated coal models incorporating both volume and CV uncertainties, and B is the number of mining blocks present in the coal model. The objective function of Equation 10 aims to maximise the total cash flow from the coal mine, whereas Equation 11 is precedence constraints, which ensure respecting the slope of the ultimate pit. For solving the optimisation formulation, the approach proposed by Asad and Dimitrakopoulos (2013) and Chatterjee et al. (2016) was used in this research to determine the mineable reserve.

Case study of an Indonesian coal mine

Study area

The research was conducted within a temporarily closed open pit situated in Indonesia. The study site is positioned approximately 150 kilometres to the north of Samarinda in East Kalimantan province and about 300 kilometres north of Balikpapan. To preserve confidentiality, the specific mine's name is withheld and will be referred to as the 'case study mine' throughout the paper. The geological characteristics of the research area, encompassing morphology, stratigraphy, geological structure, and history, define the context of the case study mine. Morphologically, the study area exhibits undulating terrain. The highest elevation reaches 325 metres above mean sea level (AMSL), while the narrow plains vary in height from 20 to 50 metres AMSL.

The study area's stratigraphy comprises the Pamaluan Formation, Balang Island Formation, and Balikpapan Formation (Figure 3). These formations harbour a substantial reserve of coal. The coal deposits took shape during the Tertiary Period within the Kutai Basin. This basin's formation is attributed to five distinct geological formations: Alluvial, Kampungbaru, Balikpapan, Pulau Balang, and Bebulu – Pamaluan. A comprehensive breakdown of each formation is depicted in Figure 3.

The predominant overburden materials encompass siltstone, mudstone, and sandstone. The thickness of the interburden remains relatively consistent. Typically, mudstone and, on occasion, carbonaceous layers are situated immediately adjacent to the coal seams. In contrast, sandstone appears discontinuously laterally, assuming a lens-shaped configuration across various dimensions. Uniaxial compressive strength (UCS) testing reveals notable discrepancies among the three materials: sandstone (19 MPa), siltstone (18.4 MPa), and mudstone (2 MPa). The average density values for sandstone, siltstone, and mudstone stand at 2.18 tonne/m^3, 2.11 tonne/m^3, and 2.07 tonne/m^3, respectively. In terms of the coal itself, its density falls within the range of approximately 1.28 to 1.32 tonne/m^3.

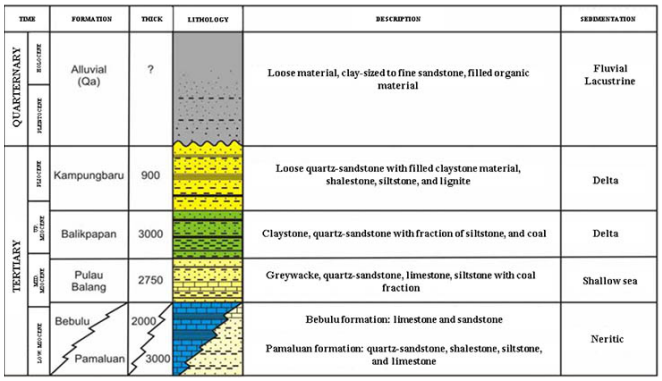

Figure 3—The stratigraphic column of the research area

Table 1

The coal quality of different coals from the case study area

Coal	Quality			
	Total moisture (%)	ASH (%)	Total sulfur (%)	CV (kcal/kg)
Prima	9–10	4–5	0.5–0.7	6,700–6,800
Pinang	13.5–15.5	5.5–6.5	0.3–0.4	6,050–6,250
Melawan	22–23	3–4	0.1–0.2	5,300–5,450

Table 2

The average coal quality parameters from different coal seams from the study area

No.	Seam	Total moisture (%)	ASH (%)	Total sulfur (%)	CV (kcal/kg)
1	P5	19.56	21.71	0.28	6,217.70
2	P4	16.10	14.32	0.60	5,651.30
3	P3	25.65	3.34	0.37	5,198.98
4	P2	12.75	26.52	0.23	5,485.42
5	P1	26.97	5.47	0.23	5,870.43
6	NU	17.51	17.88	0.35	5,653.94
7	NL	20.25	2.52	0.53	5,565.96
8	DU	17.76	10.50	0.28	5,669.70
9	B2	17.89	2.21	0.57	6,366.48
10	PRUP	18.18	25.66	0.69	6,367.12
11	PR	17.13	3.62	0.33	6,300.41
12	PRLR	16.51	8.61	0.89	6,628.91

Figure 4—The coal body model for the coal mine

Coal geology

The coal quality within the study area can be categorised into three distinct groups: Prima quality, boasting a calorific value exceeding 6700 kcal/kg; Pinang quality, characterised by a calorific value ranging from 6050 kcal/kg to 6250 kcal/kg; and Melawan quality, featuring a calorific value less than 5450 kcal/kg. This classification considers both the CV and inherent moisture (IM). Conforming to the American Society for Testing and Materials (ASTM) classification, the coal found within the study area falls under the classification of 'high volatile C bituminous coal,' encompassing an average calorific value of 5960 kcal/kg and a density of 1.3 gr/cm^3.

Table 1 provides an overview of the detailed properties of the coal extracted from the study area. Prima and Pinang coals are globally renowned for their high-quality attributes, showcasing elevated calorific values, minimal ash and sulfur content, and low water content. Prima coal is characterised by a glossy, black appearance and a notably high calorific value. Coal Pinang shares similar characteristics with Prima coal but exhibits a somewhat higher moisture content. Within the mining lease area, a total of 12 mineable coal seams are identified (PRLR, PR, PRUR, B2, DU, NL NU, P1, P2, P3, P4, and P5), and their coal properties vary reasonably within these coal seams (Table 2). The average dip of these coal seams ranges from 13.3º to 14.9º.

The simulation procedure employs a conventional deterministic coal seam model (depicted in Figure 4) as the designated training image. Geologists have meticulously crafted several strata to represent the coal deposit. The drill hole data encompasses 28 distinct lithological codes; 4 of these codes pertain to the coal zone, while the remaining 24 codes correspond to the areas outside the coal zone. A block model was formulated based on the geologist's conceptualisation. Each block within the multiple layers is either assigned as coal (1) or categorised as overburden or waste (0) for blocks located outside these layers.

The data conditioning required for simulations is sourced from 268 drill holes located within the mine lease area. The training image spans 95 x 70 x 165 blocks, each measuring 20 m^3 x 20 m^3 x 10 m^3. Referencing Figure 5, both the training image and hard data can be observed. Table 3 outlines the technical and economic parameters endorsed by the company, crucial for the reserve calculation conducted in this study. The coal reference price from the Ministry of Energy and Mineral Resources (MEMR) Indonesia has been adopted for the reserve calculation process. The MEMR

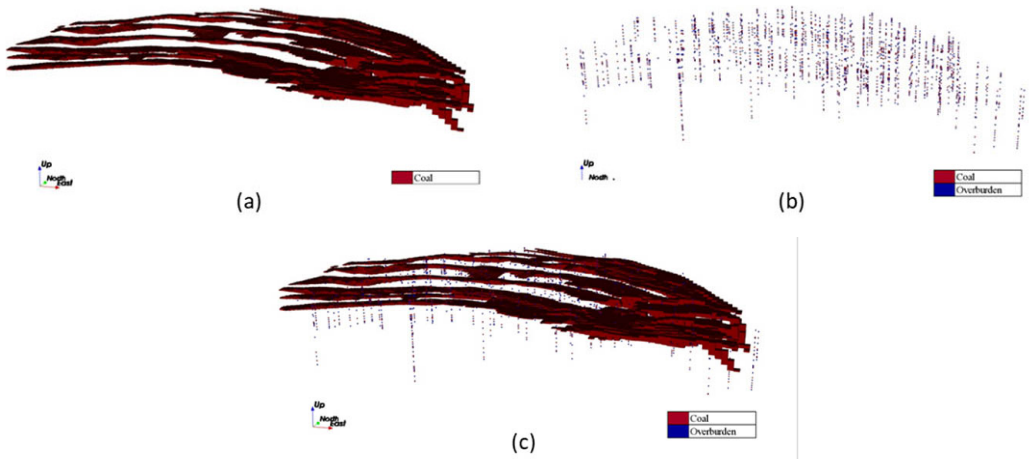

Figure 5—Visualisation of the training image and hard data: (a) training image, (b) hard data, (c) combined training image and hard data

Table 3

The technical and economic parameters used in the mine

Technical parameters	Values
Block size	20 x 20 x 10
Number of blocks	113,050
Slope constraint	45 degree
Recovery	95%
Specific gravity OB	2.1 ton/m³
Specific gravity coal	1.3 ton/m³
Economic parameters	**Values**
Mining cost OB	3 USD/tonne
Mining cost coal	0.75 USD/tonne
Washing cost coal	1.4 USD/tonne
Selling price (CV of 6322 kcal/kg GAR)	120 USD/tonne
Selling cost	2% of selling price
Discounted rate	9.5%

uses 6322 kcal/kg GAR (gross as received) CV for a reference coal price. The price for coal with a different CV was calculated using the calorific value adjustment formula, $P_{CV} = P * (\frac{CV}{6322})$, where P is the price of coal for 6322 kcal/kg GAR CV coal set by MEMR, CV is the calorific value of a given coal, and P_{CV} is the calculated coal price for coal with a calorific value of CV.

Results and discussion

Volume simulation

The SNESIM algorithm was employed to simulate the coal seams model using both the training image and the hard conditioning data (depicted in Figure 5). To accurately reproduce the coal seams' connectivity, the multi-grid method was harnessed within this study. This approach entails simulating the coarsest scale first, followed by the intermediary scale, and ultimately the finest scale. In this research, a multi-grid value of 3 was adopted, drawing from Strébelle's work in 2002 (Strebelle, 2002). A total of 20 realisations of the coal body model were generated through the SNESIM algorithm. The choice of this number was influenced by recommendations from previous researchers, as indicated by Paithankar and Chatterjee (2018). All these realisations collectively serve the purpose of quantifying geological uncertainties related to tonnage and volume.

Incorporating the entropy calculation method, as proposed by Honarkhah and Caers (2010), facilitated the optimal selection of the template size. A larger template size is intended to augment the number of nodes utilised for simulation, thereby furnishing more information to the simulated node. This strategic approach ensures that the connectivity and orientation of the geological features are accurately simulated with the available data. A sensitivity analysis of the template size calculation is provided in Table 4. In this context, the values of X and Y remain constant, while only Z varies, ranging from 3 to 13. Notably, the highest mean entropy value was observed for the 23 x 23 template size, gradually diminishing as Z increased. A marginal upswing is discerned from z = 3 to z = 5, followed by negligible increments from z = 5 to z = 13. Consequently, for the z direction, the value of 5 was chosen. Accordingly, the template size for SNESIM was established as 23 x 23 x 5.

The servo system plays a pivotal role within the SNESIM algorithm. A lower value for the servo system parameter yields a heightened proportion of the simulated primary category (coal in this instance), all while preserving the model's structure (Liu, 2006). Setting the servo system parameter to 0 signifies an absence of adjustment during simulation. As the servo number escalates, the coherence of the coal's structure diminishes, resulting in a more block-like appearance. A servo number of 1 indicates sole reliance on the training image. A sensitivity analysis of the servo number is presented in Table 5, where values indicate the coal proportion in the simulation. The coal-to-overburden (OB) ratio in the training image is approximately 0.0785, indicating about 7.8% coal and

Table 4

A sensitivity analysis of template size selection using the mean entropy calculation

	3	5	7	9	11	13	15	17	19	21	23	25	27	29	31	33	35
XY3	0.22	0.29	0.34	0.37	0.40	0.42	0.43	0.44	0.45	0.45	0.45	0.45	0.45	0.44	0.44	0.44	0.44
XY5	0.26	0.32	0.36	0.39	0.42	0.43	0.45	0.46	0.46	0.47	0.47	0.47	0.46	0.46	0.46	0.46	0.46
XY7	0.30	0.34	0.38	0.41	0.44	0.45	0.47	0.48	0.48	0.49	0.49	0.48	0.48	0.48	0.48	0.47	0.47
XY9	0.33	0.37	0.41	0.44	0.46	0.48	0.49	0.50	0.50	0.51	0.51	0.51	0.50	0.50	0.50	0.50	0.50
XY11	0.35	0.40	0.43	0.46	0.48	0.50	0.51	0.52	0.53	0.53	0.53	0.53	0.53	0.52	0.52	0.52	0.52
XY13	0.38	0.42	0.46	0.49	0.51	0.53	0.54	0.55	0.55	0.56	0.56	0.56	0.55	0.55	0.54	0.54	0.53

Table 5
Sensitivity analysis of servonumber

Simulation	Servonumber						
	0	0.5	0.6	0.7	0.8	0.9	1
1	0.087	0.080	0.077	0.074	0.074	0.074	0.078
2	0.087	0.085	0.081	0.077	0.076	0.079	0.078
3	0.085	0.082	0.079	0.074	0.072	0.074	0.078
4	0.071	0.080	0.079	0.076	0.076	0.075	0.078
5	0.080	0.084	0.082	0.080	0.078	0.077	0.078
6	0.084	0.080	0.076	0.074	0.072	0.073	0.078
7	0.069	0.079	0.078	0.075	0.075	0.073	0.078
8	0.074	0.075	0.074	0.071	0.069	0.069	0.078
9	0.087	0.081	0.078	0.074	0.070	0.078	0.078
10	0.092	0.084	0.080	0.075	0.070	0.073	0.078
11	0.076	0.080	0.076	0.073	0.070	0.074	0.078
12	0.077	0.080	0.078	0.074	0.071	0.073	0.078
13	0.084	0.078	0.076	0.074	0.075	0.075	0.078
14	0.093	0.082	0.077	0.073	0.073	0.077	0.078
15	0.086	0.083	0.081	0.077	0.075	0.075	0.078
16	0.073	0.082	0.079	0.075	0.076	0.079	0.078
17	0.071	0.083	0.081	0.077	0.077	0.075	0.078
18	0.088	0.084	0.081	0.077	0.075	0.076	0.078
19	0.072	0.076	0.076	0.072	0.073	0.074	0.078
20	0.084	0.080	0.077	0.075	0.071	0.071	0.078
Average proportion	**0.081**	**0.081**	**0.078**	**0.075**	**0.073**	**0.075**	**0.078**

92.2% overburden. The table illustrates that when the servo control parameter is set to 1, the simulation proportion mirrors the training image's proportion accurately. However, this comes at the expense of sacrificing the spatial structure of the coal seams when the servo control parameter value is large. Hence, in this study, a servo control parameter of 0.5 is adopted to preserve the coal seams' spatial structure and strike a balance between the information gleaned from the training image and hard conditioning data. Figure 6 showcases realisations of maximum, median, and minimum coal seam simulations. These images effectively capture the large-scale structures of the coal seams as depicted in the training image. Moreover, it is evident from Figure 6 (a, b, and c) that due to the inherent stochastic nature of the model, localised variations across different simulations are observable. This variability is attributed to geological uncertainty away from observation locations. It was also observed that in the central part of the deposit, there is strong agreement between the geologists' model (Figure 5) and the simulation results (Figure 6), likely due to the high density of exploration drillholes in this area. On the east and west flanks of the deposit, where drillhole density is lower, variability between the models increases. Interestingly, the western portion still shows reasonable consistency between the geological interpretation and simulations, possibly because the coal seams in this area are more continuous and clearly identifiable in the drilling records. In contrast, the eastern section exhibits the greatest discrepancies, as ambiguous seam geometry and limited data increase uncertainty in both geological interpretation and simulation outputs.

The validation of the SNESIM outcomes encompassed the calculation of overburden and coal proportions, along with experimental variograms in the X, Y, and Z directions. The proportions of simulated overburden within the models exhibited a variation ranging from 90.12% to 90.43%, considering the 20 realisations. It is noteworthy that the training image displayed an overburden proportion of 90.4%, whereas the hard data derived from drill holes featured an overburden proportion of 53.72%. Illustrated in Figure 7, the box plot depicts a minor dispersion due to the closely aligned proportions of overburden and coal among the realisations. This proximity may stem from the sedimentary deposits, which are relatively discernible through an ample volume of drilling data. The substantial similarity between the simulation and training image underscores the geologists' adeptness in interpreting coal seams with notable precision.

The variogram maps, showcased in Figure 8, affirm that the simulated coal seam effectively reproduces the spatial continuity evident in the training image across all three directions. When comparing variability, the observed disparity between the realisations and training image proves lesser than that between the realisations and hard data. This outcome was expected, as the SNESIM algorithm draws upon the patterns ingrained within the training image. It further substantiates that the algorithm does not simply generate a coal seam model that adheres to the drill hole; rather, it crafts a cohesive, interconnected, and smooth model (Goodfellow et al., 2012; Osterholt, Dimitrakopoulos, 2007; Chatterjee et al., 2012).

The realisations produced by SNESIM were harnessed to quantify the volume uncertainty within the coal deposit. The average volume for the coal seams stands at 42,505,970 m^3, accompanied by a standard deviation of 596,615.74 m^3. It is noteworthy that the average volume derived from the SNESIM algorithm surpasses (by 3.35%) that of the deterministic model

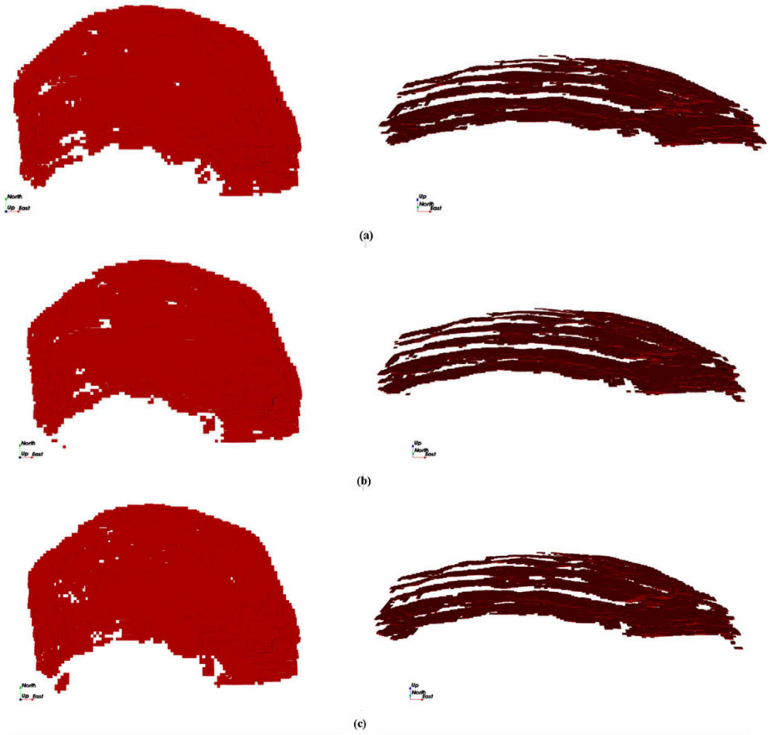

Figure 6—The simulated coal seam models (a) coal seam with maximum volume, (b) coal seam with median volume, and (c) coal seam with minimum volume

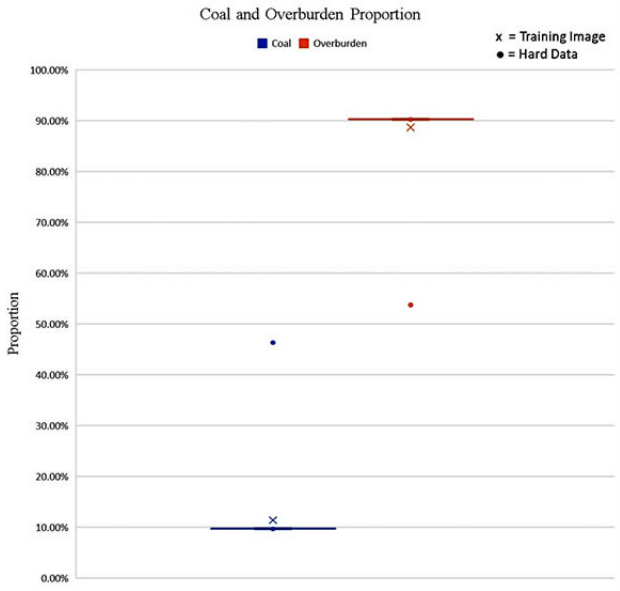

Figure 7—The box plot for coal and overburden proportion of the simulated coal seams

formulated by the geologists (41,130,000 m^3). This divergence might be attributed to the geologists' approach of simplifying the coal boundary through interpolation between drill holes, which potentially results in certain areas falling outside the delineation of coal seams. Evidently visible in Figure 5 (c), the red spot between coal layers exemplifies the geologists' attempt at achieving smooth modelling, leading to some sections at the extremities that are not adequately modelled, consequently giving rise to uncertainty.

However, it is important to note that this observation is not consistent across all 20 simulations. Among them, two instances exhibit lower volumes compared with the model devised by the geologists, with differences amounting to approximately 0.07% and 0.31%. Ultimately, the pivotal significance of these findings lies in the fact that generating multiple coal seam realisations facilitates a quantifiable assessment of volume uncertainty risk within the coal deposit. The subsequent phase involves translating this volume uncertainty into the realm of calorific value (CV) uncertainty within the coal deposit, enabling a comprehensive evaluation of both these uncertainty factors in tandem.

Calorific value simulation

To quantify calorific value (CV) uncertainty within the coal seam model, each individual SNESIM realisation is treated as a distinct coal seam model. The SGS is then employed to estimate coal CV values based on the drill hole data. Prior to delving into variogram modelling and SGS, the composited CV data undergo a transformation into normal scores, resulting in the establishment of a Gaussian distribution characterised by a mean of zero and unit variance. Subsequently, variogram models are developed for SGS, employing a lag distance of 20 m, tolerance of 10 m, angular tolerance of 45°, and bandwidth of 22.5 m.

In the pursuit of accurate modelling, experimental variograms are calculated across three directions and juxtaposed with fitting theoretical models. Figure 9 graphically portrays these experimental variograms and the corresponding fitted theoretical models along the three distinct directions. The fitted model notably indicates that the coal deposit exhibits geometrical anisotropy, as described in the work of Isaaks and Srivastava (1989). This insight informs the development of a combined variogram model, which is subsequently employed for the CV simulation. Detailed specifications of this combined variogram model can be found in Table 6.

Within each SNESIM realisation of coal seams, a total of fifty simulations were conducted to determine coal CV values. Notably,

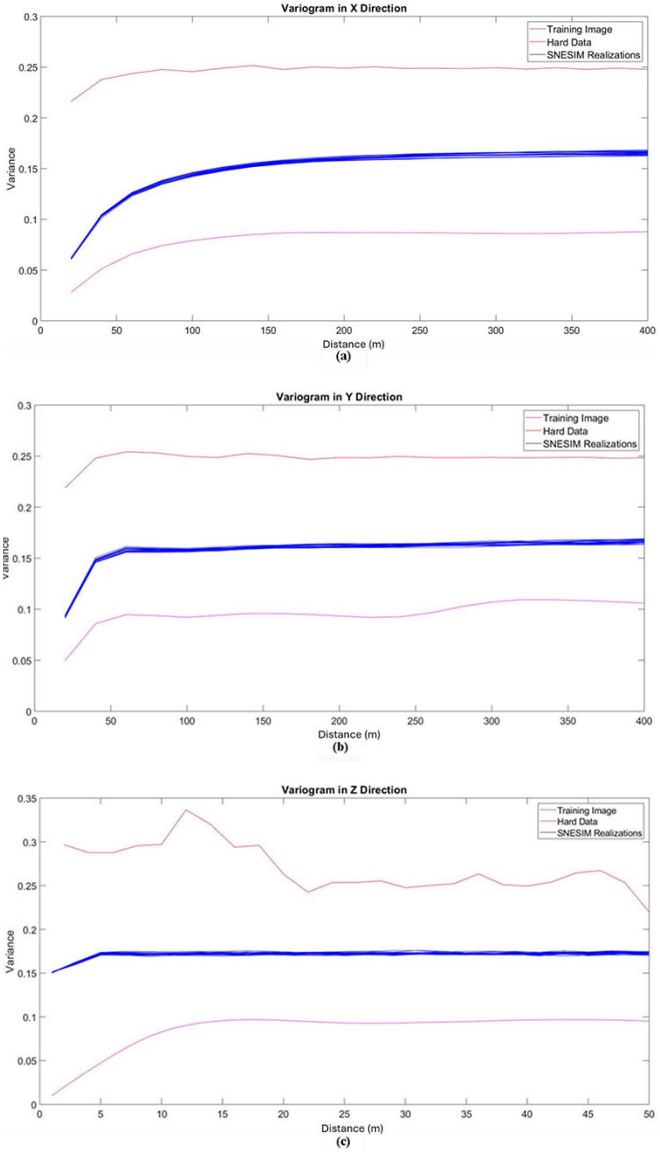

Figure 8—The variograms of the simulated coal seams models (a) variogram in X-direction, (b) variogram in Y-direction, and (c) variogram in Z-direction

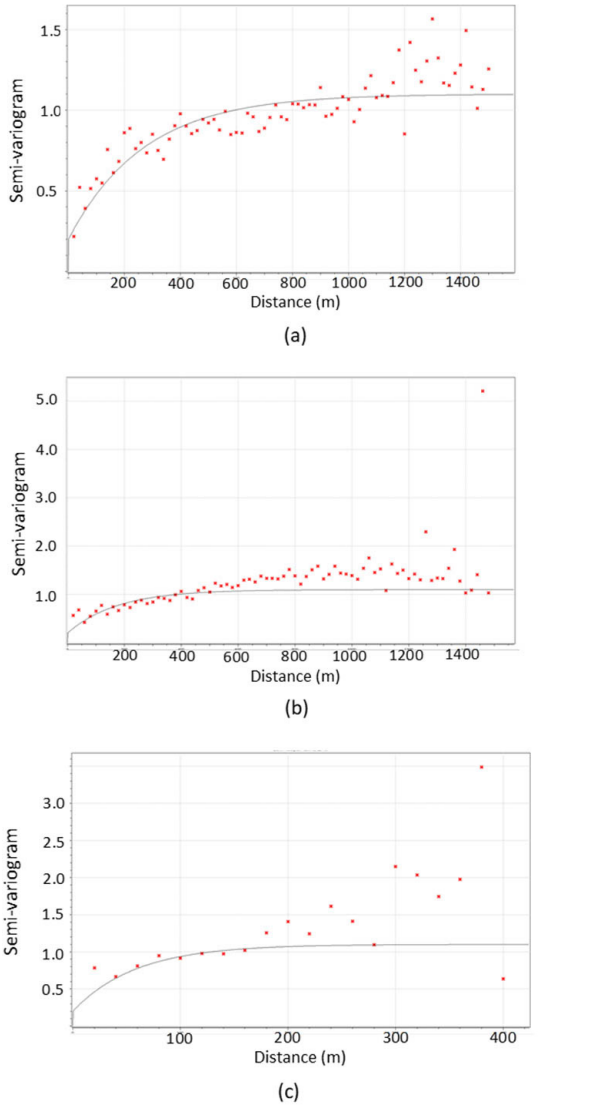

Figure 9—Variogram of the normal score CV data along (a) X - direction, (b) Y - direction, and (c) Z - direction

these simulations were performed independently for each distinct coal seams model. Once the CV simulation phase concluded, the resulting realisations underwent a back transformation process to revert to the original data space. As depicted in Figure 10, a top-view representation illustrates two coal CV realisations across three distinct volume simulations. An overarching observation gleaned from all realisations is the notable contrast between the southern and northern sides of the deposit in terms of CV values. Further insights are gleaned from Figure 11, which provides a north-east section view of the coal seams simulations. Here, it becomes evident that the deeper coal seams exhibit higher CV values relative to their shallower counterparts.

The spatial simulation of CV reveals consistent spatial patterns across the three coal volume models (maximum, median, and minimum). As shown in top-view (Figure 10), higher CVs are consistently observed in the southern part of the study area, whereas the eastern region shows lower CVs across all simulations. However, the central portion exhibits greater variability in calorific value, indicating higher uncertainty in this zone. This is consistent with the statistics observed from the exploration

Table 6
Combined variogram model of the normal score CV data

Variogram model	Major (x)		Minor (z)	
	Azimuth	Dip	Azimuth	Dip
$\gamma(h) = 0.2 + 0.8\gamma_1\left(\sqrt{\left(\frac{h_x}{810}\right)^2 + \left(\frac{h_y}{525}\right)^2 + \left(\frac{h_z}{176}\right)^2}\right)$	90°	0°	0°	-90°

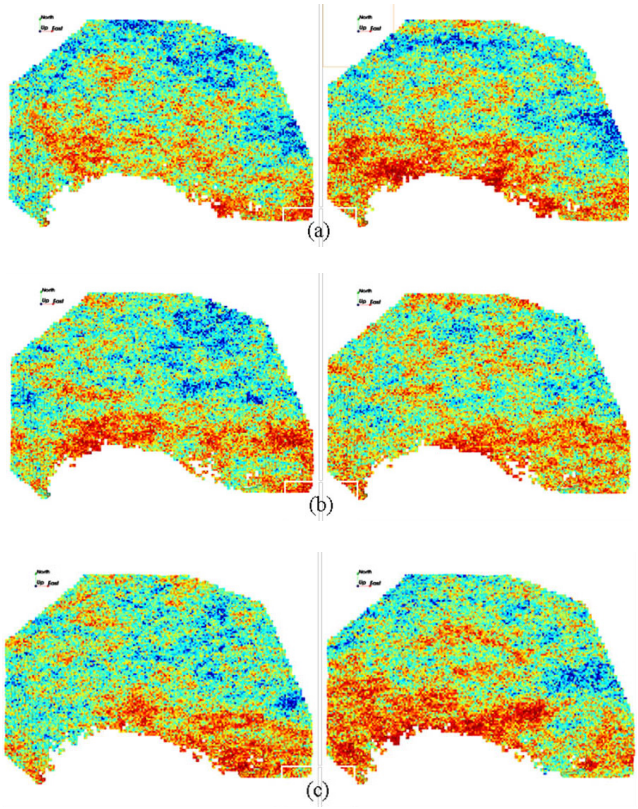

Figure 10—Top view for coal CV simulations (kcal/kg) in (a) coal seams model with maximum volume, (b) coal seams model with median volume, and (c) coal seams with minimum volume

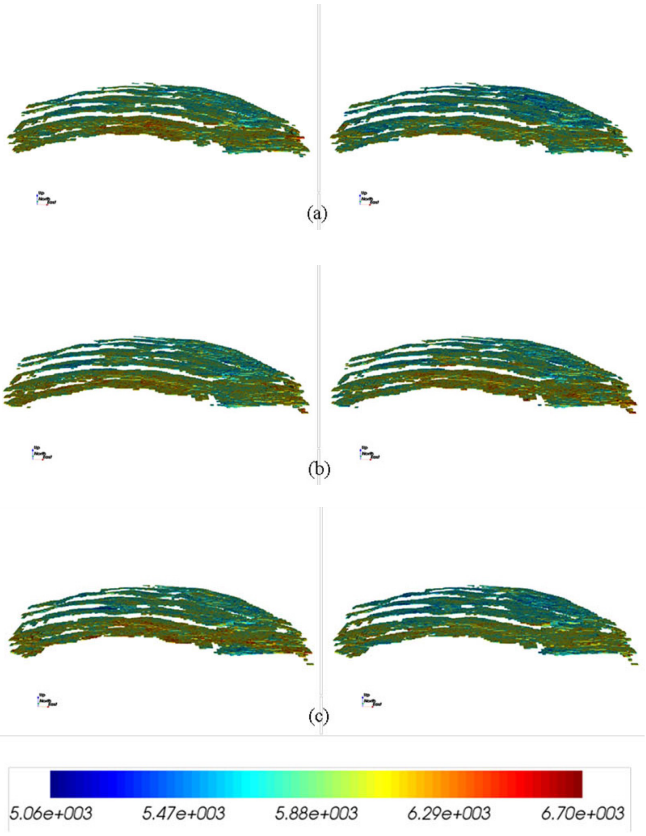

Figure 11—North-east view of coal CV simulations (kcal/kg) in (a) coal seams model with maximum volume, (b) coal seams model with median volume, and (c) coal seams model with minimum volume

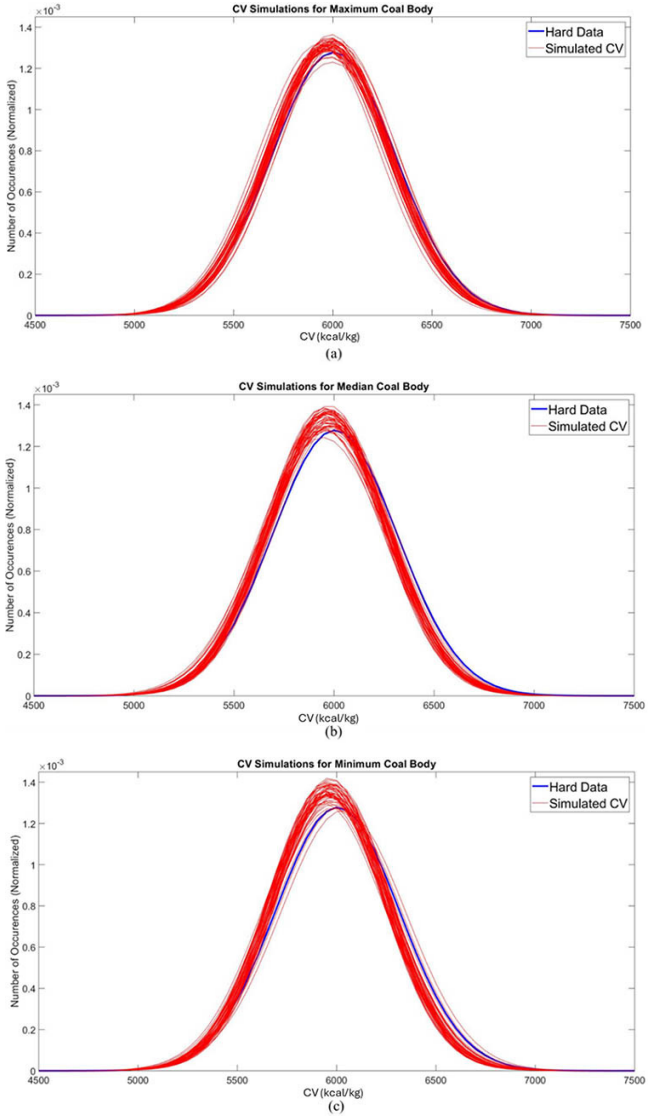

Figure 12—The histograms of the coal CV simulations in (a) coal seams with maximum volume, (b) coal seams with median volume, and (c) coal seams with minimum volume

drilling data: although the central part has a higher density of drillholes, the variance among samples is also higher due to the presence of multiple overlapping seams with distinct calorific value characteristics. From the side-view simulations (Figure 11), it is evident that the deeper seams generally exhibit higher calorific values. Specifically, seams B2, PRUP, PR, and PRLR, located near the bottom of the stratigraphic sequence, show elevated average CVs, as also reflected in Table 1. These seams register average calorific values of 6,366.48 kcal/kg, 6,367.12 kcal/kg, 6,300.41 kcal/kg, and 6,628.91 kcal/kg, respectively, the highest among all seams analysed. Additionally, increased variability in CV is observed in the western region, primarily attributed to the sparse distribution of exploration samples in that area, which limits confidence in the simulation outputs.

To validate the coal CV simulations, histograms and experimental variograms of the realisations were generated, thereby affirming the accurate reproduction of both first- and second-order statistical characteristics. Illustrated in Figure 12, histograms provide a visual comparison between the drill hole data and the coal CV simulations for coal seams. Figure 13 presents the variograms

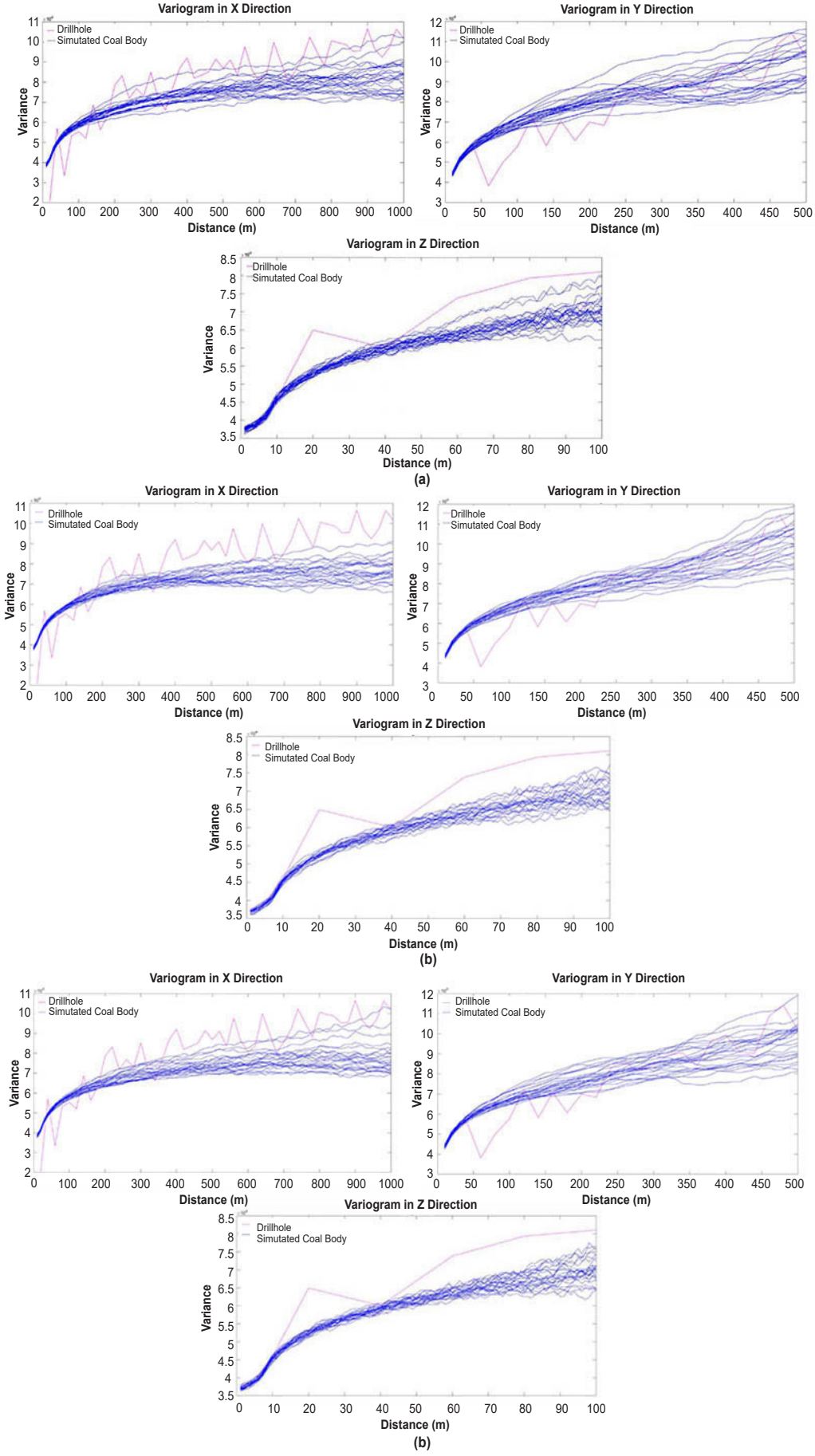

Figure 13—The variograms for estimated coal CV in (a) coal seams with maximum volume, (b) coal seams with median volume, and (c) coal seams with minimum volume

Table 7
The volume and CV summary results

Realisation number	Coal volume m³	Min average estimated CV (kcal/kg)	Max average estimated CV (kcal/kg)
real1	43,384,400	5,305.26	6,484.14
real2	41,100,200	5,322.41	6,490.77
real3	41,998,800	5,312.98	6,495.53
real4	42,363,200	5,354.81	6,506.92
real5	42,824,800	5,348.89	6,505.53
real6	42,802,400	5,329.10	6,492.22
real7	42,893,600	5,378.11	6,518.51
real8	43,065,200	5,344.97	6,500.56
real9	42,451,600	5,332.98	6,496.25
real10	42,198,800	5,354.66	6,503.78
real11	42,608,800	5,334.37	6,495.48
real12	42,606,400	5,383.71	6,526.55
real13	42,604,000	5,337.54	6,500.94
real14	43,024,400	5,345.20	6,490.09
real15	42,750,000	5,370.37	6,504.78
real16	41,001,200	5,322.43	6,482.74
real17	42,126,000	5,333.81	6,494.67
real18	42,787,200	5,338.02	6,491.53
real19	42,700,800	5,349.92	6,507.20
real20	42,827,600	5,327.40	6,496.48

corresponding to the coal CV simulations and the drill hole data. In all instances, the outcomes effectively capture the spatial attributes inherent in the original data, further consolidating the reliability of the coal CV simulations.

Table 7 succinctly presents the synthesised outcomes of volume and CV uncertainties. The tabulated information encompasses 20 simulated coal body models, delineating the range between minimum and maximum averaged simulated CV values within the coal seams. To ascertain this range, the minimum and maximum averages of CV are deduced from the culmination of 50 Gaussian simulations within each coal seam simulation, followed by an averaging process specific to each simulation. This collective data portray an average CV fluctuating between 5,305 kcal/kg and 6,526 kcal/kg. In juxtaposition, the deterministic scenario hinges upon a single geologist-derived model, relying on ordinary kriging for single-grade estimation. This deterministic perspective, as depicted in Table 8, facilitates an overarching estimation for mean CV and standard deviation within the blocks constituting the coal geobody. While contrasting the standard deviation, Table 8 underscores the reference standards of the conventional coal seams model, prepared by geologists. The application of ordinary kriging, known for its status as the best linear unbiased estimator (BLUE), underpins this reference. The results gleaned from Table 8 show a standard deviation of 222.78 for the conventional model, whereas the simulated volume and CV model manifest a standard deviation of 586.54. The disparity in standard deviations can be attributed to the integration of hard data (drill hole) projections within the coarsest grid during simulation. This amalgamation leads to the compromise of local accuracy, a phenomenon acknowledged in the work of Painthankar and Chatterjee (2017), who encountered analogous findings during simulations for a copper deposit. Coincidentally, Bastante et al. (2008) also corroborated these

Table 8
The statistics of the two estimation methods

Method	CV mean (kcal/kg)	Standard deviation (kcal/kg)
Ordinary kriging (OK)	5,986.76	222.78
SNESIM + SGS	5,920.29	586.54

observations, mirroring the results reported by Painthankar and Chatterjee (2017), although their study involved the utilisation of SNESIM, indicator kriging, and sequential indicator simulation for a slate deposit.

Illustrated in Figure 14 is the distribution function of the two models under consideration. Notably, the ordinary kriging model with the geologist-prepared coal seams model exhibits a propensity for greater clustering around the mean, effectively reducing the variability of the CV. This observation aligns with expectations, given the inherent smoothing nature of kriging, which serves to mitigate error variance. In contrast, the distribution function emanating from the SNESIM and SGS models portrays a more consolidated tendency towards the upper limit of CV values. This effect, likely, is a result of the conditional independence intrinsic to both the SNESIM and SGS approaches, thereby fostering a more pronounced concentration of CV values at the higher end of the spectrum.

Coal reserve calculation

Following the quantification of resources involving volume and CV uncertainties, the derivation of the ultimate pit limit was undertaken to compute the mineable reserve. In this stochastic model, all pertinent uncertainty factors, encompassing volume

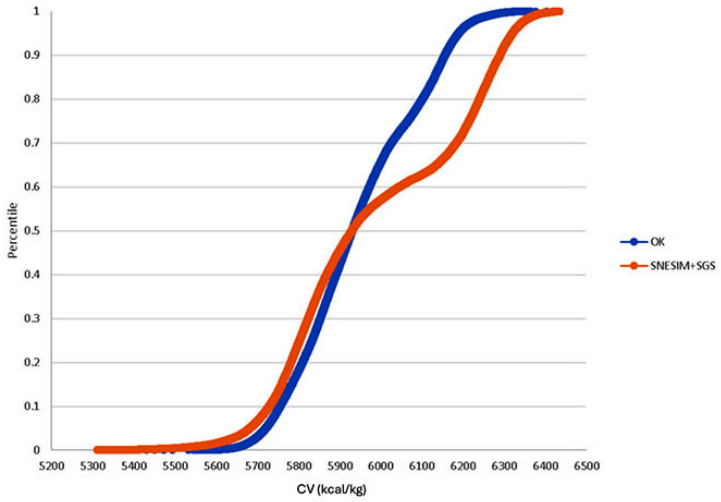

Figure 14—The distribution functions of the CV frequencies from two different model

Table 9

Risk profile of the mineable reserve within ultimate pit

Method	Total blocks	Coal quantity (million tons, MT)			CV (kcal/kg)		
		Min	Med	Max	Min	Med	Max
Stochastic mineable reserve	67,026	175.4	182.7	185.6	5,150.34	6,019.66	6,766.98
Deterministic mineable reserve	66,946	182.4			5,913.7		

and CV, were meticulously accounted for. The coal seams model (volume) was subjected to simulation across 20 realisations, and each of these simulated coal seams models were further imbued with 50 realisations of calorific value simulations, culminating in a total ensemble of 1,000 combinations (50 x 20 = 1,000). Employing the stochastic maximum-flow minimum-cut approach, the calculation of the ultimate pit limit was executed.

This modelling strategy coherently integrates the diverse realisations of coal volume and the estimated CV of mining blocks, enabling the generation of block economic values (BEVs). Subsequently, a singular graph was constructed employing the procedural methodology outlined in Chatterjee et al. (2016) and Asad and Dimitrakopoulos (2013). The ultimate pit limit determination abides by the stipulations of Equations 10 and 11 to furnish a solution. Within this purview, the total number of blocks encompassed by the ultimate pit limit amounted to 67,026.

For the computation of coal reserves, the focus was directed towards the 67,026 blocks situated within the confines of the ultimate pit. A risk analysis of coal tonnage and calorific value across 1,000 realisations was carried out, and the results are summarised in Table 9. The stochastic reserve model estimates the minimum, median, and maximum coal tonnage as 175.4 MT, 182.7 MT, and 185.6 MT, respectively. The corresponding CV ranges from a minimum of 5,150.34 kcal/kg to a median of 6,019.66 kcal/kg and a maximum of 6,766.98 kcal/kg. The tonnage stripping ratio (waste to ore) calculated using the specific gravity of coal and overburden (as shown in Table 3) ranges from 1.41 to 1.59 (minimum: 1.41, median: 1.46, maximum: 1.59). A comparative analysis was executed between the conventional (deterministic) and stochastic methodologies for ultimate pit limit generation. In the stochastic paradigm, multiple realisations of coal volume and CV are synergistically combined, contrasting with the deterministic approach that exclusively relies upon a solitary model of volume and CV. The distinct coal volume model was procured from the geologist-designed coal seams model, while the CV was ascertained via kriging algorithm (Goovaerts, 1997). Uniform parameterisation was maintained across both approaches.

Table 9 additionally encapsulates the outcomes of the ultimate pit limit for the deterministic model. The results show that the tally of blocks (coal + overburden) is marginally lower in the deterministic model compared with the stochastic model. Specifically, the block count within the deterministic model accounts for 66,946, constituting a diminutive 0.2% disparity in relation to the stochastic model. However, the tonnage stripping ratio in the deterministic model is very similar to the median value of the stochastic counterpart, quantifying at 1.46. An intriguing observation that can be made from the data is that the average CV yielded by the stochastic model (6,019.66 kcal/kg) reasonably surpasses the average CV value arising from the deterministic model (5,913.7 kcal/kg).

For the computation of undiscounted cash flow across the mine's operational lifespan, the BEV for each block situated within the ultimate pit was aggregated. The risk profile encompassing the undiscounted cash flow arising from the stochastic model of the mineable reserve is outlined in Table 10. An examination of the data reveals that, on average, the case study mine possesses the potential to generate approximately USD47,141.2 million, utilising the stochastic model that incorporates both volume and CV uncertainties. A comparative analysis against the deterministic model exposes a significant finding: the stochastic model yields

Table 10

Risk profile of undiscounted cash flow within ultimate pit

Method	Undiscounted cash flow (USD in million)		
	Minimum	Average	Maximum
Stochastic mineable reserve	37,696.4	47,141.2	55,264.1
Deterministic mineable reserve	42,771.3		

a 12% increment in undiscounted cash flow extracted from the mineable reserve of the deposit. This augmentation can be attributed to the stochastic model's inclination towards the extraction of mining blocks characterised by higher CV values (as depicted in Table 9) throughout the mine's operational tenure. As a natural consequence, this propensity culminates in the generation of a heightened economic value (as detailed in Table 10) when juxtaposed with the deterministic model.

Conclusions, limitations, and future research

For any coal mining project, the primary objective is to design a mine that optimises revenue generation. Accurate estimation of coal volume and CV is paramount, as over- or underestimations of these factors can significantly impact the project's feasibility and success. Therefore, incorporating these uncertainties into the reserve calculation can allow coal mine planners to strategically devise a mining plan. This paper introduces a systematic approach to assess the uncertainties related to coal volume and calorific value using a case study of a coal mine in Indonesia. The methodology employs geostatistical techniques to assess volume and CV uncertainties within coal seams. This involves creating a series of equiprobable coal seam models through simulation. SNESIM's flexibility in data conditioning and its ability to mimic common shapes found in coal geological formations make it an ideal choice. The uncertainty pertaining to CV is evaluated through SGS. The process involves generating 20 SNESIM realisations to account for coal volume uncertainty. Within each of these realisations, 50 SGS instances are generated to capture the variability in CV. The validity of these realisations is confirmed by their ability to replicate relevant statistical parameters. The reserve estimation using these simulation models by the stochastic model shows the average stripping ratio is 1.46 and the average calorific value is 6019.66 kcal/kg. In comparison to the deterministic model, the stochastic reserve model generates an average of 10% more undiscounted cashflow. Nonetheless, a risk assessment reveals that the optimistic solution yields 29% more undiscounted cashflow, whereas the pessimistic solution generates 12% less from the mineable coal reserve compared with the deterministic estimate. Hence, a meticulous analysis of uncertainties associated with estimating mineable reserves offers enhanced decision-making insights for coal mining projects.

One of the key limitations of this study is that it considers only geological uncertainty in the coal reserve estimation process. In practice, several other variables, such as coal price, mining costs, coal washing costs, and pit slope angle, also exhibit significant uncertainty and can substantially impact reserve estimates and economic outcomes. Apart from geological uncertainties (coal volume and calorific value), this study assumes that all other parameters remain constant throughout the mine's life cycle. Future research will aim to incorporate these additional sources of uncertainty into the reserve estimation framework. Furthermore, production scheduling, which sequences mining activities and enables the calculation of year-by-year cash flows, will also be developed to account for these uncertainties, thereby providing a more comprehensive and realistic evaluation of project performance.

References

Abulkhair, S., Madani, N. 2022. Stochastic modeling of iron in coal seams using two-point and multiple-point geostatistics: A case study. *Mining, Metallurgy & Exploration,* vol. 39, no. 3, pp.1313–1331.

Afzal, P. 2018. Comparing ordinary kriging and advanced inverse distance squared methods based on estimating coal deposits; case study: East-Parvadeh deposit, central Iran. *Journal of Mining and Environment*, vol. 9, no. 3, pp.753–760.

Amini, S.H., Vass, C., Shahabi, M. Noble, A. 2022. Optimization of coal blending operations under uncertainty–robust optimization approach. *International Journal of Coal Preparation and Utilization*, vol. 42, no. 1, pp. 30–50.

Arpat, G.B., Caers, J. 2007. Conditional simulation with patterns. *Mathematical Geology*, vol. 39, pp.177–203.

Asad, M.W.A., Dimitrakopoulos, R. 2013. Implementing a parametric maximum flow algorithm for optimal open pit mine design under uncertain supply and demand. *Journal of the Operational Research Society*, vol. 64, no. 2, pp. 185–197.

Bastante, F.G., Ordóñez, C., Taboada, J., Matías, J.M. 2008. Comparison of indicator kriging, conditional indicator simulation and multiple-point statistics used to model slate deposits. *Engineering Geology*, vol. 98, no. 1–2, pp. 50–59.

Camus, J.P. 2002. *Management of mineral resources: creating value in the mining business*. SME.

Chatterjee, S., Dimitrakopoulos, R., Mustapha, H. 2012. Dimensional reduction of pattern-based simulation using wavelet analysis. *Mathematical Geosciences*, vol. 44, pp. 343–374.

Chatterjee, S., Sethi, M.R., Asad, M.W.A. 2016. Production phase and ultimate pit limit design under commodity price uncertainty. *European Journal of Operational Research*, vol. 248, no. 2, pp. 658–667.

CIM. 2014. Nobody likes surprises: The role of the Certified Cost Professional. CIM Magazine. November, 2014. http://www.cim.org/en/Publications-and-Technical-Resources/Publications/CIM-Magazine/2014/November/columns/Finance.aspx(last access on August 23, 2023).

Deutsch, C.V., Journel, A.G. 1992. Geostatistical software library and user's guide. *New York*, vol. 119, no. 147, p. 578.

Dimitrakopoulos, R., Godoy, M. 2014. Grade control based on economic ore/waste classification functions and stochastic simulations: examples, comparisons and applications. *Mining Technology*, vol. 123, no. 2, pp. 90–106.

Dimitrakopoulos, R., Li, S.X. 2010. Quantification of fault uncertainty and risk assessment in longwall coal mining: stochastic simulation, back analysis, longwall design and reserve risk assessment. *Mining Technology*, vol. 119, no. 2, pp. 59–67.

Dimitrakopoulos, R., Farrelly, C.T., Godoy, M. 2002. Moving forward from traditional optimization: grade uncertainty and risk effects in open-pit design. *Mining Technology*, vol. 111, no. 1, pp. 82–88.

Godoy, M., Dimitrakopoulos, R. 2011. A risk quantification framework for strategic mine planning: Method and application. *Journal of Mining Science*, vol. 47, pp. 235–246.

Goodfellow, R., Consuegra, F.A., Dimitrakopoulos, R., Lloyd, T. 2012. Quantifying multi-element and volumetric uncertainty, Coleman McCreedy deposit, Ontario, Canada. *Computers & Geosciences*, vol. 42, pp. 71–78.

Goovaerts, P. 1997. *Geostatistics for natural resources evaluation*. Oxford University Press, USA.

Heriawan, M.N., Koike, K. 2008. Uncertainty assessment of coal tonnage by spatial modeling of seam distribution and coal quality. *International Journal of Coal Geology*, vol. 76, no. 3, pp. 217–226.

Hochbaum, D.S. 2001. A new—old algorithm for minimum-cut and maximum-flow in closure graphs. *Networks: An International Journal*, vol. 37, no. 4, pp. 171–193.

Honarkhah, M., Caers, J. 2010. Stochastic simulation of patterns using distance-based pattern modeling. *Mathematical Geosciences*, vol. 42, pp. 487–517.

Huang, T., Lu, D.T., Li, X., Wang, L. 2013. GPU-based SNESIM implementation for multiple-point statistical simulation. *Computers & geosciences*, vol. 54, pp. 75–87.

Journel, A., Zhang, T. 2006. The necessity of a multiple-point prior model. *Mathematical geology*, vol. 38, pp. 591–610.

Kumar, A., Chatterjee, S. 2017. Open-pit coal mine production sequencing incorporating grade blending and stockpiling options: An application from an Indian mine. *Engineering optimization*, vol. 49, no. 5, pp. 762–776.

Liu, Y. 2006. Using the Snesim program for multiple-point statistical simulation. *Computers & geosciences*, vol. 32, no. 10, pp. 1544–1563.

Moore, T.A., Friederich, M.C. 2021. Defining uncertainty: Comparing resource/reserve classification systems for coal and coal seam gas. *Energies*, vol. 14, no. 19, p. 6245.

Osterholt, V., Dimitrakopoulos, R. 2007. Simulation of wireframes and geometric features with multiple-point techniques: application at Yandi iron ore deposit. *Orebody modelling and strategic mine planning*, 2nd edn. AusIMM, Spectrum Series, 14, pp. 95–124.

Paithankar, A., Chatterjee, S. 2018. Grade and tonnage uncertainty analysis of an African copper deposit using multiple-point geostatistics and sequential Gaussian simulation. *Natural Resources Research*, vol. 27, pp. 419–436.

Pyrcz, M.J., Deutsch, C.V. 2014. *Geostatistical reservoir modeling*. Oxford University Press, USA.

Rendu, J.M. 2002. Geostatistical simulations for risk assessment and decision making: the mining industry perspective. *International Journal of Surface Mining, Reclamation and Environment*, vol. 16, no. 2, pp. 122–133.

Saikia, K., Sarkar, B.C. 2013. Coal exploration modelling using geostatistics in Jharia coalfield, India. *International Journal of Coal Geology*, vol. 112, pp. 36–52.

Siddiqui, F.I., Pathan, A.G., Ünver, B., Tercan, A.E., Hindistan, M.A., Ertunç, G., Atalay, F., Ünal, S., Kıllıoğlu, Y. 2015. Lignite resource estimations and seam modeling of Thar Field, Pakistan. *International Journal of Coal Geology,* vol. 140, pp. 84–96.

Sohrabian, B., Soltani-Mohammadi, S., Tercan, A.E. 2023. Joint simulation of coal quality attributes using a new simulated annealing-based method of diagonalisation. *International Journal of Mining, Reclamation and Environment*, vol. 37, no. 3, pp. 216–242.

Stevanović, D.R., Kolonja, B.M., Stanković, R.M., Knežević, D.N., Banković, M.V. 2014. Application of stochastic models for mine planning and coal quality control. *Thermal Science*, vol. 18, no. 4, pp. 1361–1372.

Strebelle, S. 2002. Conditional simulation of complex geological structures using multiple-point statistics. *Mathematical geology*, vol. 34, pp. 1–21.

Strebelle, S.B., Journel, A.G. 2001, September. Reservoir modeling using multiple-point statistics. *In SPE Annual Technical Conference and Exhibition?* (pp. SPE-71324). SPE.

Tercan, A.E., Sohrabian, B. 2013. Multivariate geostatistical simulation of coal quality data by independent components. *International Journal of Coal Geology*, vol. 112, pp. 53–66.

Tercan, A.E., Ünver, B., Hindistan, M.A., Ertunç, G., Atalay, F., Ünal, S., Kıllıoğlu, Y. 2013. Seam modeling and resource estimation in the coalfields of western Anatolia. *International Journal of Coal Geology*, vol. 112, pp. 94–106.

Wang, S., Cao, B., Bai, R. Liu, G. 2025. Determination of production capacity for open-pit coal mines under uncertainty: A model based on economies of scale. *PloS one*, vol. 20, no. 1, e0312130.

Yüksel, C., Benndorf, J., Lindig, M., Lohsträter, O. 2017. Updating the coal quality parameters in multiple production benches based on combined material measurement: a full case study. *International Journal of Coal Science & Technology*, vol. 4, pp. 159–171.

Zhang, Y., Underschultz, J., Langhi, L., Mallants, D., Strand, J. 2018. Numerical modelling of coal seam depressurization during coal seam gas production and its effect on the geomechanical stability of faults and coal beds. *International Journal of Coal Geology*, vol. 195, pp. 1–13. ◆